Weakly-Supervised Crack Detection

Yuki Inoue and Hiroto Nagayoshi

Abstract—**Pixel-level crack segmentation is widely studied due to its high impact on building and road inspections. Recent studies have made significant improvements in accuracy, but overlooked the annotation cost bottleneck. To resolve this issue, we reformulate the crack segmentation problem as a weakly-supervised problem, and propose a two-branched inference framework and an annotation refinement module that requires no additional data, in order to counteract the loss in annotation quality. Experimental results confirm the effectiveness of the proposed method in crack segmentation as well as other target domains.**

Index Terms—**Crack detection, weak supervision, semantic segmentation, retinal blood vessel segmentation, deep learning.**

I. INTRODUCTION

KEEPING roads crack-free is crucial for public safety, as cracks are first signs of structural deterioration, and they may lead to more severe problems such as potholes and collapses. As such, automatic crack detection is a critical responsibility of transportation departments.

Crack detection problem is typically formulated as a semantic segmentation problem, as it is crucial to gather information about various crack properties such as width and orientation in addition to location to accurately assess the conditions of the target structure [1]–[5]. Such analysis is impossible with other problem settings like object detection and image classification. However, one major bottleneck with semantic segmentation is the annotation cost, as pixel-level annotation is one of the most cost-intensive annotations to obtain. In addition, it is not ideal to reuse a model across different sites, as the appearance of a crack varies greatly across environments and materials of the target structure, further increasing the annotation burden. As transportation departments must often maintain various types of structures like roads, bridges, and buildings under diverse environments, minimization of annotation cost is crucial for practical crack detection systems.

Unfortunately, although there have been many studies on improving the detection accuracy of crack detectors [1]–[5], few deals with the annotation cost. In the earlier version of this manuscript [6], we proposed to use imprecise annotations during model training, *i.e.* formulate the problem as a weakly-supervised problem. While imprecise annotations significantly reduced the preparation cost, they lead to imprecise model training. In order to counteract the negative effects of the low quality annotations, we introduced a two-branch detection framework. In the proposed framework, we complement a conventional data-driven inference model (named *Macro Branch*)

with a rule-based inference path named *Micro Branch*. The Micro Branch was based on a simple rule-based method that exploited the fact that crack pixels are generally darker than their surroundings. Although we showed in [6] that this simple heuristic is effective in many situations, its domain-specific nature posed two problems for robust inference. First, we showed in the same paper that it does not work well for lighter-colored cracks. Additionally, our further experimentation in this paper reveals that it does not generalize well to non-crack targets, because the brightness profile is not as simple.

Recognizing these problems with our earlier work, this version makes several new contributions. First, we refine the annotations before they are used to train the Macro Branch. This is done by taking advantage of the fact that the regions falsely annotated as cracks should have similar local visual features as the background. As annotation refinement is adjusted according to the dataset it is applied, we hypothesize that the annotation refinement module leads to a more robust performance compared to the pixel darkness-based Micro Branch, which bases its decisions on a static rule independent of the dataset characteristics. Second, we empirically confirm this hypothesis through thorough experimentations on various crack datasets, including ones that contain lighter-colored cracks. In addition, we conduct experiments on the retinal blood vessel segmentation task and show that while the effectiveness of pixel darkness strategy depends on domains, the annotation refinement strategy consistently improves the inference performance.

II. RELATED WORK

A. Annotation Efficient Semantic Segmentation

In general semantic segmentation literature, various forms of annotations have been tried to replace the expensive pixel-level annotation.

One way to provide annotation is through point supervision, in which a small number of pixels in the form of scribbles are annotated for each object. Bearman *et al.* [7] accomplished this by predicting the objectness score. Boykov *et al.* [8] proposed an interactive model that utilizes the GrabCut algorithm [9] to segment objects with scribbles.

Another way to provide annotation is through bounding boxes. For example, Khoreva *et al.* [10] devised a method based on GrabCut to clean the bounding box information for pixel-level annotation.

Some studies attempted segmentation by utilizing image labels. Most of them first identify rough object locations with a class activation map (CAM) such as Grad-CAM [11] and refines the CAM result afterward. For example, Kolesnikov *et al.* [12] designed three novel losses to expand the initial CAM prediction and refine the result with conditional random fields, and Ahn *et al.* [13] predicted a displacement field and class boundary map to determine the boundary of the CAM output.

Y. Inoue and H. Nagayoshi are with the Center of Artificial Intelligence, Hitachi Ltd, Tokyo, Japan, (e-mail: yuki.inoue.wh@hitachi.com, hiroto.nagayoshi.wy@hitachi.com).

Unfortunately, many of the aforementioned methods do not translate well to the crack detection task due to the geometry of cracks. For example, shifting to point supervision does not significantly reduce the annotation burden, because cracks can be as narrow as one pixel. Also, bounding box supervision is not appropriate, as cracks may appear diagonally in an image. In such a case, a bounding box will mostly contain background, making training inefficient. Axis un-aligned bounding boxes may be effective to a some degree, but it still struggles to annotate cracks that branch out in multiple directions. Furthermore, there often exist multiple interpretations of one, contiguous crack entity. For example, it is non-trivial to identify the endpoints of a crack, making bounding box annotation inconsistent among annotators. On the other hand, methods based on CAM can be made suitable for crack detection, when combined with proper post-processing, as discussed in Sec. II-B.

B. Annotation Efficient Crack Detection

Let us restrict our search for annotation reduction efforts in crack detection literature. Generally speaking, there are unsupervised, weakly-supervised, and semi-supervised approaches.

Rule-based crack detectors can be thought of as unsupervised methods as they do not require explicit annotations. Unfortunately, they often require experts to tune the parameters when adapting to new environments, which could be problematic. In addition, rule-based approaches are known to be inferior in performance when compared to data-driven counterparts [2], [3]. More recently, data-driven methods such as ones based on auto-encoders [14], [15] and Generative Adversarial Networks [16] are used for unsupervised anomaly detection, which could be viewed of as a generalized case of unsupervised crack detection. In many of these methods, models learn to reconstruct non-defective images. Crack detection is achieved through the model's inability to accurately reconstruct the anomaly images.

In weakly-supervised settings, approximate annotations are provided. There are two ways of weakly-supervised crack detection, differing in the format of the supervision. First provides supervision in the form of classification labels. Cracks are subdivided into patches, and each patch is annotated whether it contains any cracks. We will refer to this as *patch-level weak supervision*. Fan *et al.* [17] was one of the first to try this approach, training a classifier model with the weak labels and applying a rule-based thresholding method for patches in which the trained classifier predicted as containing cracks. One major disadvantage of their proposal is that the supervised model can only isolate the crack regions up to rectangular patches. Because cracks are thin, these selected patches mostly contain non-crack regions and are difficult to be refined. König *et al.* [18] and Dong *et al.* [19] improved the approach by refining the patch-level estimation of the classifier with gradient activation maps, similar to the method mentioned in previous section. The CAM outputs are refined by thresholding methods such as conditional random field or Otsu's binarization.

We proposed in [6] another form of weak-supervision, an imprecise semantic segmentation annotation as illustrated in Fig. 1. This is based on the observation that much of the

(a) Precise annotation.
B: true crack,
W: true non-crack.

(b) LQ annotation.
B: LQ crack,
W: LQ non-crack.

(c) Superposed.
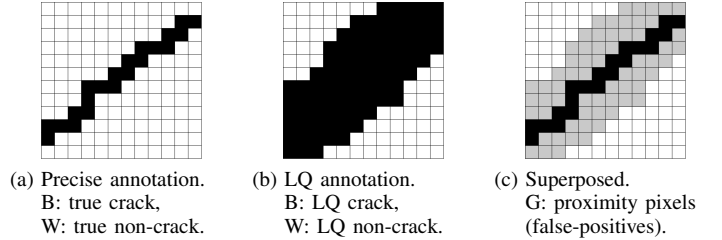G: proximity pixels
(false-positives).

Fig. 1. Illustrations of weakly-supervised annotation. Each cell represents a pixel. *LQ* in the captions stand for low quality, and *B*, *W*, *G* stand for black, white, and gray pixels, respectively.

TABLE I
DATASET INFORMATION AND ANNOTATION TIMES. NOTE THAT ONLY CFD WAS RE-ANNOTATED PRECISELY FOR TIME MEASUREMENT. *Precise*, *Rough*, AND *Rougher* CORRESPOND TO TYPES OF ANNOTATIONS, DETAILS DESCRIBED IN SEC. IV-A1.

Dataset	Sample counts		Annotation time per image (sec.)		
	Train	Test	Precise	Rough	Rougher
Aigle	24	14	-	34	23
CFD	71	47	656	70	22
DCD	300	237	-	97	17

annotation time is spent on investigating border pixels between crack and non-crack regions, so annotation duration can be greatly reduced by allowing the annotator to ignore the crack boundary. As summarized in Table I, up to 96% of the annotation time was saved with this annotation strategy. We will refer to this as *pixel-level weak supervision*.

Semi-supervised learning, in which a fraction of images is precisely annotated while others are left without annotations, is another form of an annotation-efficient training strategy. However, semi-supervised approach is not popular in crack detection literature, because precise annotations take disproportionately longer time than weak annotations. This is because most of the annotation time is spent on judging where the crack boundaries are, as the boundaries between crack and non-crack regions are often blurry and ambiguous. In addition, even after the boundaries are determined, they are tedious to annotate, because boundary lines are often complex. With a weak annotation, the annotators can ignore both of these difficulties.

Ultimately, pixel-level weak supervision is chosen as the mode of annotation in our paper. In the next section, we will discuss the pros and cons of each approach as well as the reason for the final selection.

III. PROPOSED METHOD

A. Annotation Design Choice

This section will describe why we chose the pixel-level weak supervision over other forms of annotations.

First, the unsupervised approach was not selected because although the performances of unsupervised methods have improved in the past years, they are still inaccurate compared to supervised counterparts. For example, Duan *et al.* and Mubashshira *et al.* [20], [21] either perform marginally better than rule-based methods or worse than the supervised methods. On the other hand, Yu *et al.* [16] claim that their unsupervised model outperforms all supervised models under all datasets,

except against FPHBN model evaluated on the CRACK500 dataset [2], in which it underperforms by 5.5%. However, this claim is slightly misleading. First, out of the 8 models compared, only FPHBN can be considered a competitive model by today's standards. In addition, the performance values of FPHBN is taken from the original paper [2], which obtains the result by training FPHBN with CRACK500 and evaluating it across different datasets. In other words, all results of FPHBN except for CRACK500 are out-of-domain results not suitable for a fair comparison, at least for our purposes. Comparing the results for CRACK500, we conclude that supervised model still outperforms the unsupervised ones. Drops in performance can lead to cracks being overlooked, which in turn may lead to serious accidents. So if the small cost of creating rough annotations can significantly improve performance, it should be strongly preferred.

We mentioned in Sec. II-B that unsupervised crack detection can be viewed as a special case of unsupervised anomaly detection. However, anomaly detectors may not always replace crack detectors, as most unsupervised methods in the field of anomaly detection [14], [15] train the models to detect *any unforeseen differences* from the images they are trained with, rather than detecting a specific anomaly target, *i.e.* cracks in our case. This means that if we want to ignore certain defect types, their samples must be included in the training dataset, so that the model learns to ignore them. For example, if a model should not detect rust, images of rusted objects must be present in the training dataset in a sizeable volume. This targeted sample collection process could take more than the annotation process itself, potentially negating the benefits of the unsupervised approach.

Second, patch-level weak supervision was not selected because it is not efficient compared to pixel-level weak supervision. For example, in König *et al.*'s approach [18], each image is subdivided into patches of $32{\times}32$ pixels, at a stride of 16 pixels. Considering that the images used for training are roughly $400{\times}400$ pixels, approximately 600 image-level annotations are needed for each image. How these image patches are annotated is not described in the paper, as the image-level annotations are likely automatically calculated from the pixel-level annotations that came with the dataset. Probably the most efficient method to annotate such a collection of image patches is to present the whole image with $16{\times}16$ pixel grids showing the patch boundary as shown in Fig. 2b, and ask the annotators to choose patches that contain cracks. As the patch size is relatively small, the annotators must carefully follow the paths of the cracks as they select the patches. This is very similar to how annotation is done for pixel-level weak supervision, except that cracks are annotated in free-form, as shown in Fig. 2c instead of in grid-form. As annotation process is very similar to each other, we assume that their time efficiency is also similar.

However, patch-level weak annotations contain less information for training. As patch-level annotations are built on a grid of super-pixels, they are better interpreted as spatially-discretized version of pixel-level annotations. Fig. 2 shows an example of the two annotations for the same crack, and we can see that the patch-level annotation lacks details compared to the pixel-level counterpart. It may be more intuitive to think

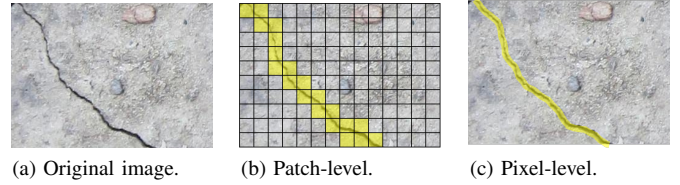(a) Original image. (b) Patch-level. (c) Pixel-level.

Fig. 2. Comparisons between the two types of the weak supervision annotations. The yellow region represents the annotated crack region. The time efficiencies of the two methods are similar, althogh patch-level weak supervision is a discretized version of the pixel-level weak supervision.

about how two annotation forms can be converted to each other. Converting from pixel-level annotations to patch-level annotations can easily be done by aggregating pixel information in each of the super-pixel cells, while the opposite conversion is not possible. This is because pixel-level annotations contain all information that patch-level annotations contain, but not vice versa. Therefore, we decided to formulate crack detection as a pixel-level weakly-supervised problem.

B. Pixel Darkness Assisted Inference

Formulating crack detection as a pixel-level weakly-supervised problem implies that the annotation labels contain mistakes, mostly concentrated near the crack boundaries. Therefore, a crack detector must be able to recover the boundary information lost during the annotation process. To do so, we observed how human annotators annotate cracks and noticed that the annotation process is typically done in two steps. First, an annotator determines the rough locations of cracks by examining the entire image. Then, the annotator zooms into a section, compares its pixel darkness against its neighbors, and annotates dark pixels as cracks.

Our framework shown in Fig. 3 in blue, first proposed in [6], emulates these two steps. First, rough localization of cracks is achieved via *Macro Branch*, a supervised segmentation model trained on the low quality (LQ) annotations. Fine details of cracks lost during the annotation process are then recovered by the *Micro Branch*, which is implemented as a simple per-pixel darkness calculation. The outputs of two branches are aggregated by a pixel-level multiplication and thresholded to produce the final output. As any off-the-shelf semantic segmentation model can take the role of the Macro Branch, any existing crack detection system can easily adopt this framework.

C. Annotation Refinement

A major shortcoming of the two-branch inference strategy is that as the annotation quality degrades, the ability of the Macro Branch to locate the cracks degrades proportionally, and it becomes too challenging for the Micro Branch to accurately recover the crack details. Since the rule-based Micro Branch heavily depends on the fact that cracks are dark, this problem is more prominent for datasets that contain cracks of lighter colors. One way to remedy this situation is to regain the Macro Branch's ability to locate cracks by somehow improving the annotation quality. In this paper, we introduce an annotation refinement process that requires no further additional information, as summarized in Fig. 3 in green.
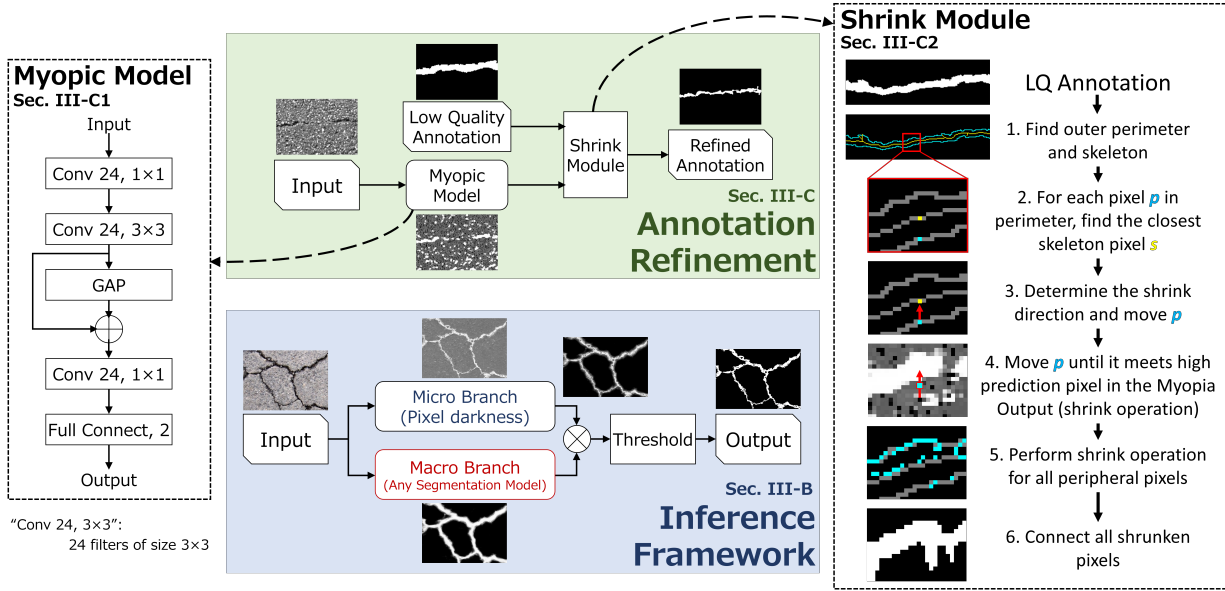
Fig. 3. Overview of the proposed framework. The annotation refinement is done with a receptive field limited Myopic Model, and the inference framework emulates the local and global attention strategies annotators naturally take during annotation.

1) Myopic Models: At first glance, we are tasked with an impossible problem: how can the quality of the LQ annotation be improved, if no extra information is available? To analyze this problem, let us investigate the LQ annotations in a closer detail. To avoid confusions, the crack and non-crack regions of the precise annotation will be referred to as *true crack* and *true non-crack* regions, and that of the LQ annotation as *LQ crack* and *LQ non-crack* regions.

Fig. 1 illustrates an example of fully-supervised (Fig. 1a) and weakly-supervised (Fig. 1b) annotations for the same crack. Each grid cell in the figure represents a pixel. As illustrated in the figure, because annotators are instructed to over-annotate, LQ crack pixels are composed of two types of pixels: those that are truly cracks and false-positive pixels that surround them (proximity pixels). Note that false-negative pixels are not considered because they occur so rarely under the over-annotation setting. In order to improve the quality of the LQ annotation, a model must classify true crack pixels as cracks and proximity pixels as non-cracks. What makes this difficult is the fact that proximity pixels are annotated as cracks in the LQ annotation. As most typical models have large enough receptive fields to judge if a pixel is in proximity of true crack pixels, models learn to classify proximity pixels as cracks, which is undesired. The problem here is that a model has too large of a receptive field. So we instead design a segmentation model with a small receptive field, so as to restrict it from being able to access the proximity information. Because of this short-sighted nature, we name this model the *Myopic Model.*

Because Myopic Models do not have the access to the proximity information, they should not be able to differentiate between proximity pixels and LQ non-crack pixels, as the two regions have similar local appearances (since they both do not contain cracks). This results in conflicting backpropagation updates generated by two similarly appearing inputs. However, because there are more LQ non-crack pixels than proximity

pixels, the backpropagation signals from the LQ non-crack pixels dominate. As a result, the Myopic Models correctly learn to classify proximity pixels as non-cracks, contrary to what LQ annotation dictates.

In our implementation, the Myopic Model is implemented as a simple three-layer CNN as shown left of Fig. 3, with a receptive field of size 3×3. Note that as long as the receptive field size is kept small, other forms of implementations such as support vector machines and decision tree-based methods may be just as effective. CNN is chosen merely due to its simplicity in implementation.

To further strengthen the ability of the Myopic Model to ignore mislabels during training, the cross-entropy loss is modified as shown in Eq. 1. In the equation, x is a pixel in an image, p_x is the predicted crack probability at x, H represents the set of pixels in an LQ crack region with crack probability in the top 90 percentile, and B represents the set of pixels in an LQ non-crack region with crack probability in the bottom 90 percentile. The added conditions (in colors) will be referred to as the ignore conditions, as they force the model to ignore its low predictions in the crack regions (red) and high predictions in the non-crack regions (blue).

$$L_{CE} = -\sum_{x \in H} \log(p_x) - \sum_{x \in B} \log(1 - p_x) \qquad (1)$$

2) Shrink Module: In our problem setting, annotation refinement equates to reducing the number of false-positive pixels, as false-negative pixels are assumed to be minimal. This can be achieved by utilizing the mislabel-ignoring nature of the Myopic Models. However, we empirically observed that a simple application of the Myopic Model not only removes false positives from the annotation but also removes true crack pixels from the annotation, introducing false negatives. The false negatives typically break continuities of crack regions,

which is detrimental during training. In order to preserve continuity, we introduce the Shrink Module.

Assuming that true crack pixels are concentrated near the center of the LQ crack regions, annotation can be refined by *shrinking* the contours of the LQ crack regions. As outputs of a Myopic Model provide good indications of where true crack pixels are, they can be used to guide the shrinking process. In addition, because this shrink procedure preserves the cracks' continuity, it should produce better refinement results than simply using the Myopic Model's output as the refined annotation.

The right side of Fig. 3 summarizes the details of the Shrink Module. The process starts by determining which pixels in the LQ crack annotation L the shrink operation should be applied to, by calculating the outer contour pixels[1] P (step 1). Then, the shrink direction v is calculated from the closest point between $p \in P$ and skeletonized pixel[2] $s \in S$ (steps 2 and 3). Then, each p is moved in v direction until it meets pixels with high probability in the Myopic Model output M (step 4, *shrink operation*). "High probability" is defined as the case in which the probability value of M at the new pixel is higher than that at the original contour coordinate by a threshold. To reduce noise, the shrink operation continues until the condition is met twice in a row.

The shrink operation is performed for all p to form the refined set R (step 5). If the criteria is not met for a particular p, its starting coordinate is added to R. The final refined image is generated by connecting the pixels in R and filling the resulting contour.

Finally, the step-by-step procedure of the proposed framework is summarized below:

1) Train a Myopic Model f_{mm}, using LQ annotation D_{lq} (Sec. III-C1)
2) Generate refined annotations D_{ref} from the outputs of f_{mm} and D_{lq}, via Shrink Module (Sec. III-C2)
3) Train a Macro Model f_{macro} using D_{ref}
4) Perform inference using f_{macro} and f_{micro} (rule-based darkness calculation, Sec. III-B)

D. Pixel Darkness vs. Annotation Refinement

We would like to conclude this section by comparing the pixel darkness approach (Sec. III-B) and the annotation refinement process (Sec. III-C).

In both methods, certain inductive biases about the segmentation target are made in order to recover the target boundary information lost during the imprecise annotation process. The pixel darkness based approach assumes that the targets are darker, which is highly effective for finding cracks, but highly inflexible as the decision logic is fixed regardless of the target. On the other hand, the data refinement approach makes three assumptions about the target: (1) the background region is significantly larger than the target region (2) the target has small chromatic variation (3) the target is long and connected. The first two assumptions are utilized in designing the Myopic Model and the last assumption is utilized in designing the Shrink Module. These assumptions are more general than the

---

[1] Calculated via *findContours* function in OpenCV package [22].
[2] Calculated via *skeletonize* function in scikit-image package [23].

pixel darkness assumption, as it is valid for any thin targets, not just for cracks. Furthermore, the chromatic properties of the target is learned from the dataset by the Myopic Model, making it more robust to different targets.

IV. EXPERIMENTS

A. Dataset

The Aigle dataset (Aigle) [24], Crack Forest dataset (CFD) [25], and DeepCrack dataset (DCD) [3] are used for evaluation. As shown in Fig. 4, characteristics of cracks vary greatly across datasets. For example, Aigle has a complex backgound, CFD's cracks are the least distinct, and DCD contains the thickest cracks. In addition to the precise annotation provided with the datasets (Precise Annotation), two types of imprecise annotations, manual and synthetic, are prepared.

1) Manual Annotation: Manual annotations are annotated by a human annotator and there are two types: Rough and Rougher, with Rougher lower in quality. The annotation rules provided to the annotator are as follows (values in {} correspond to rules for the Rough Annotation, and [] correspond to rules for the Rougher Annotation):

> Set the size of the pen tool to be {1 or 2} [3 or 4] pixels larger than the average width of the cracks. You are allowed to adjust it {as many times as needed} [once at most] per image. Trace the cracks in one stroke unless the crack width is larger than the pen size, and {follow as much as possible} [ignore] the small contours. For thicker cracks (approx. 8 pixels or wider), use a pen size of {4} [8] pixels to trace the outline. Fill it with a bucket tool afterward.

The time taken for annotation are summarized in Table I. Note that the annotation times for the Precise Annotation are unknown, so CFD was re-annotated precisely for approximation. As the table shows, it took an order of magnitude shorter to annotate the Rough and Rougher Annotations than to annotate the Precise Annotation. This also supports our choice of weakly-supervised learning over semi-supervised learning, as the time devoted to annotate the Rougher Annotation for CFD is only enough to precisely annotate 4 images, which is likely too small for effective training.

2) Synthetic Annotation: In addition to the manual annotations, a suite of synthetic annotations is machine-generated from the Precise Annotation using image dilation and deformation. The synthesized annotations are prepared for three reasons. First, the annotation quality is easily quantifiable and controllable by the number of dilations. Second, the synthesis pipeline can arbitrarily be extended to obtain annotations of various quality at a small cost. Finally, it is void of any biases that a human annotator may introduce.

The detail of the synthesis pipeline is outlined in Alg. 1. First, a Precise Annotation sample p is dilated n_{dil} times to generate a dilated sample d (steps 4-5). This n_{dil} value dictates the quality of the resulting annotation. Examples of p and d are shown in the left column of Fig. 5 as white and green regions, respectively. To test the proposed framework under various settings, 4 annotations with different n_{dil} are synthesized ($n_{dil} \in \{1, 2, 3, 4\}$). Then, Elastic Transform [26] is applied to the
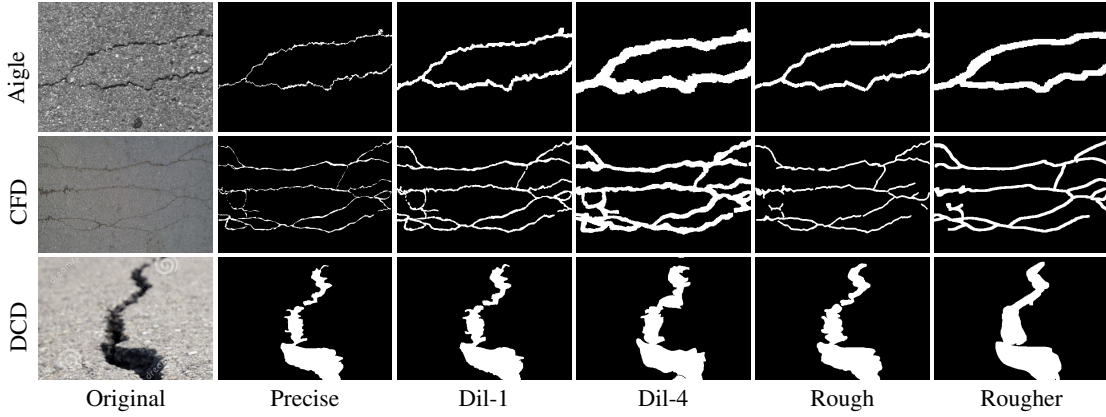
Fig. 4. Annotation samples (white pixels: crack, black pixels: non-crack). Taken from [6]. Dil-1 and Dil-4 correspond to synthetic annotations with 1 and 4 dilations during the synthesis process, respectively.

Algorithm 1: Annotation Synthesis Procedure

```
Input  : P                // Precise Annotations
         n_dil    // Number of dilation to apply
Output : S                // Synthesized Annotations
1  S ← ∅ forall p ∈ P do
2  |   α_L ← 10
3  |   α_U ← 10000
4  |   repeat n_dil times
5  |   |   d ← Dilate(p)
6  |   repeat
7  |   |   α ~ U(α_L, α_U)
8  |   |   s ← ElasticTransform(α, d)
9  |   |   r ← Recall(s, p)        // Calculate recall
10 |   |   if r ≥ 0.975 then
11 |   |   |   α_L ← α
12 |   |   if r ≤ 0.925 then
13 |   |   |   α_U ← α
14 |   until 0.925 ≤ r ≤ 0.975
15 |   S ← s
16 return S
```
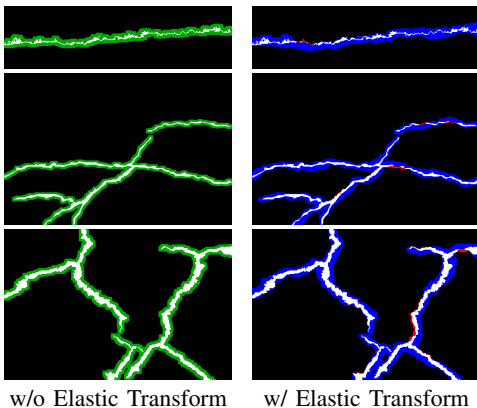

Fig. 5. Dilation Annotation synthesis process (for dilation=4). Precise Annotation (white) is dilated (green) and distorted by Elastic Transform (blue). Note that the Dilation Annotation is synthesized so that it does not fully contain the Precise Annotation. The false negative pixels are in red.

dilated sample to form a synthesis candidate s (step 8). This image deformation step ensures that the true crack region does not always lie in the center of the synthesized weak annotation.

Examples of s is shown in the right column of Fig. 5 as blue regions. Elastic Transform implementation in Albumentations [27] has three parameters: α, σ, alpha_affine. σ is fixed at 12 to prevent excessive deformation, and alpha_affine is fixed at 0.2. Finally, s and p are compared by calculating the recall value r (step 9). In order to emulate rushed human annotators, this calculated recall value should neither be too high nor too low. For the annotations generated for the paper, the upper and the lower bounds are chosen to be 0.975 and 0.925, respectively (step 14). Relationships between values of α and recall vary greatly across different images, so α is searched randomly from a uniform distribution (step 7), with the range initialized to be between 10 to 10000 (steps 2-3), and narrowed according to the obtained recall value (steps 10-13).

B. Evaluation Metrics

The models are evaluated using the Optimal Dataset Scale (ODS), as defined in Eq. 2, where P_i^t and R_i^t represent the precision and recall values at threshold t, of the i-th image in the dataset with N samples. Since what follows the maximum operator is the definition of the F1-score, ODS is essentially F1-score optimized for the best threshold value to be used in a dataset. Note that pixel tolerances typically introduced to absorb the annotation inaccuracies ([1], [28]) are not used because it ambiguates the effect of LQ annotations.

$$ODS = \max_{0<t<1} \frac{1}{N} \sum_{i=1...N} \frac{2P_i^t R_i^t}{P_i^t + R_i^t} \quad (2)$$

C. Macro Branch Implementations

Four semantic segmentation models are tested as the Macro Branch to assess the versatility of the proposed framework.

a) MIL-CD [1]: The model proposed by Inoue *et al.* achieved high performances for Aigle and CFD. It consists of 7 convolutional layers with around 12 filters each, and it is augmented by the Multiple Instance Learning (MIL) architecture, which calls for the inference to be performed twice, rotating the image by $0°$ and $90°$. To avoid confusion, we will refer to this model as MIL Crack Detector (MIL-CD).
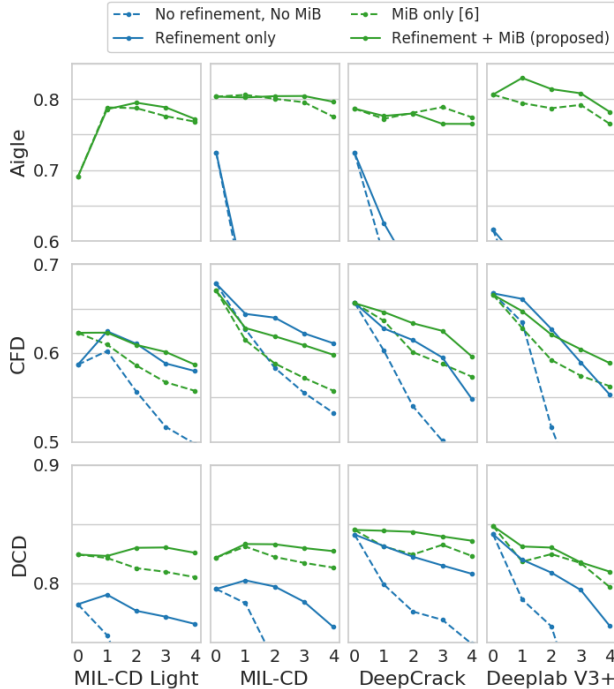
(a) Results on the synthetic annotation. Horizontal axis: annotation quality, lower the value, higher the quality. *0* corresponds to the Precise Annotation.
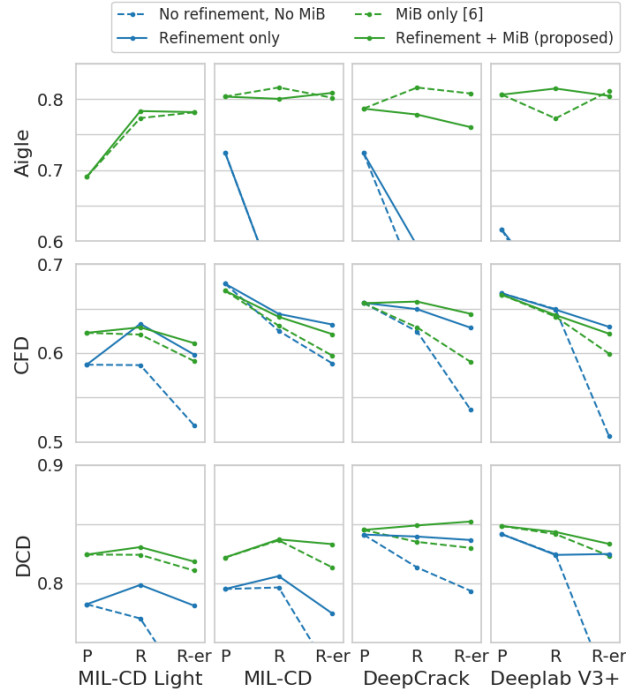
(b) Results on the manual annotation. P: Precise, R: Rough, and R-er: Rougher Annotations.

Fig. 6. Evaluation results on different LQ annotations. For all plots, annotation quality decreases from left to right. MiB represents cases in which the Micro Branch is included during inference.

b) MIL-CD Light: A computationally lighter version of MIL-CD is also tested to evaluate the effectiveness of the framework for extremely light models. This model also has 7 convolutional layers, but *CONV 2* and *CONV 4* layers have strides of 2 instead of 1, the number of filters at each layer is halved, and the MIL configuration is not used.

c) DeepCrack [3]: The model proposed by Liu *et al.* achieved high performance for DCD. It employs encoder-decoder architecture with skip connections, and its inner feature representations are supervised at different stages to better capture information from multiple scales[3].

d) DeepLab V3+ [29]: This model is one of the state-of-the-art model architectures for the general semantic segmentation task. It employs both spatial pyramid pooling as well as encoder-decoder architecture to capture multi-scale information. Note that this model is by far the most computationally heavy model among the tested models[4].

D. Results

1) Evaluation on the Low Quality Annotations: The results of the proposed framework on weak supervision are summarized in Fig. 6. The colors of the plots correspond to the presence of the Micro Branch, and the solid and dotted lines correspond to the inclusion of the annotation refinement step. Note that what we proposed in [6] corresponds to dotted green lines. The plots indicate that annotation refinement improves

[3]Implementation adopted from https://github.com/yhlleo/DeepSegmentor
[4]Implementation adopted from https://github.com/tensorflow/models/
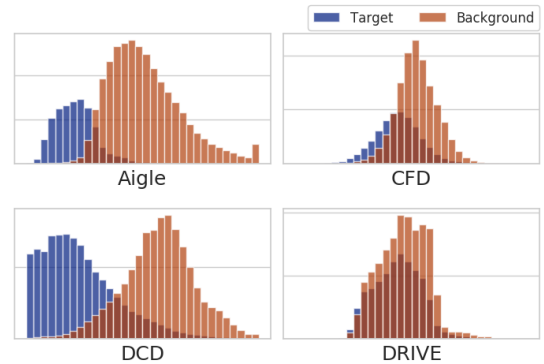

Fig. 7. Brightness distribution of the pixels included in the positive regions of Rougher Annotation.

model performance for most datasets and models, confirming its robustness. In addition, annotation refinement is effective regardless of Micro Branch presence, which means that the two methods improve the performance independently. The average improvements achieved by including the annotation refinement module, over all models and annotations, are 0.3% for Aigle, 2.5% for CFD, and 1.1% for DCD, meaning that the annotation refinement module improved the model performance the most for CFD, in which the Micro Branch struggled the most.

On the other hand, the performance improvement was minimal for Aigle. This is likely a by-product of the Micro Branch's unrealistic success on Aigle. As Fig. 7, which summarizes the pixel brightness distributions of true crack and
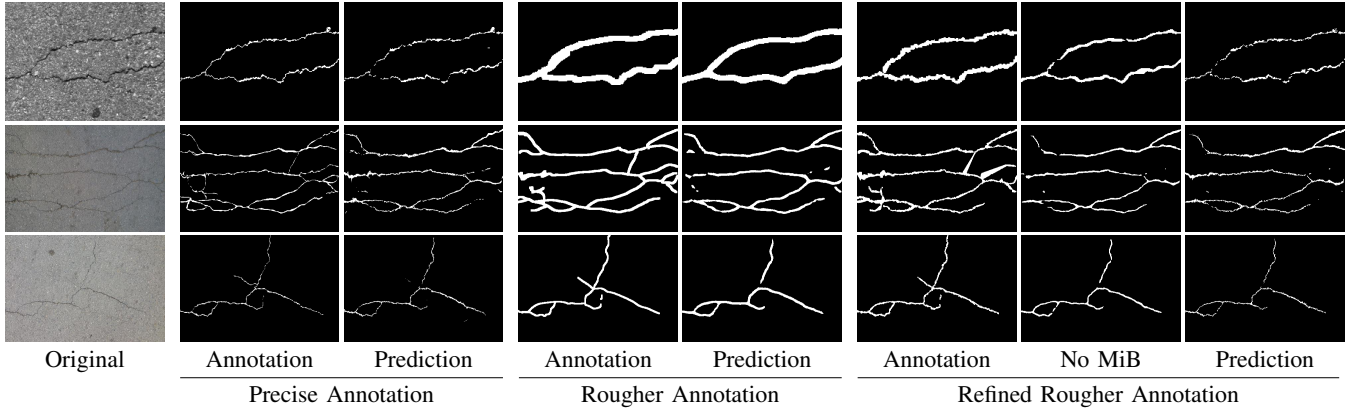
Fig. 8. Sample predictions of the DeepCrack model under fully-supervised and weakly-supervised settings. MiB stands for the Micro Branch.

true non-crack pixels included in the LQ crack regions of the Rougher Annotation, shows, brightness distributions of the two regions are well separated for Aigle. As a result, the pixel darkness strategy works extremely well for Aigle, implying that the Micro Branch can better select crack pixels from the Macro Branch outputs. Under this situation, it becomes more advantageous for the Macro Branch have a high recall rather than a high precision, as false positives have distinct brightness profiles and are easy to remove. Therefore, it becomes better for the Macro Branch to over-detect. This can be confirmed from Fig. 6, as the performance of models with no annotation refinement sometimes improves for annotations of slightly lower quality (*i.e.* the Rough and Dil-1 Annotations) for Aigle. This is because although the Macro Branch tend to over-detect when trained with lower quality annotations, it works in favor overall, because the Micro Branch can remove false-positives so effectively. Conversely, annotation refinement, which improves precision at a cost of recall, hurts the overall performance when used in conjunction with the Micro Branch for Aigle.

On the other hand, the brightness distribution is overlapping for CFD. As a result, the Micro Branch struggles to improve performance. Overlapping brightness distribution is less detrimental for the annotation refinement module, as it is data-driven and can adapt to dataset characteristics. Fig. 6 shows that the annotation refinement only method in solid blue lines outperforms the Micro Branch only method in dotted green lines.

Samples of annotation refinement and inference for Deep-Crack are shown in Fig. 8. As expected, models trained with less precise annotations learn to predict less precisely. The low precision output is greatly improved after the annotation is refined using the method described in Sec. III-C2. Finally, the inclusion of the Micro Branch further improves the prediction.

V. ADDITIONAL EXPERIMENTS

A. Ablation Studies

Table II summarizes the ablation results. All experiments are conducted with DeepCrack. The first two rows in the table correspond to *Refinement only* and *MiB only* plots in Fig. 6, respectively, and they show that (1) including Micro Branch is
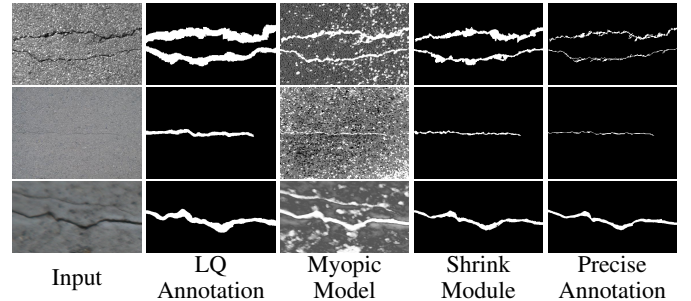

Fig. 9. Examples of annotation refinement process.

important and (2) annotation refinement is effective for CFD and DCD, as discussed in Sec. IV-D1.

a) Ignore Condition: The ignore condition is introduced to help the model ignore mislabels by removing high crack predictions in LQ non-crack regions and low crack predictions in LQ crack regions from the loss function. Table II shows that the ignore condition is the most effective for Aigle. One explanation for this is that backgrounds in Aigle images have highly complex textures (Fig. 4 shows an example). Therefore, it should be nearly impossible for the Myopic Model to tell the difference between the complex background textures and crack regions, as it only receives highly localized input. The introduction of the ignore condition allows the Myopic Model to drop the incorrect backpropagation signals generated by the complex-textured backgrounds.

b) Shrink Module: As shown in Fig. 9, the outputs of the Shrink Module contain fewer false positives than the LQ annotation. In addition, they are more connected than the Myopic Model outputs, and are overall more similar to the ground truth.

The effect of the annotation refinement methods on the annotation quality is also visualized in Fig. 10, which plots the recall and precision of the unrefined annotation (Unrefined), the annotation in which only the Myopic Model is applied (Pre-shrink), and the annotation in which the Shrink Module is applied (Shrink), indicated by different shapes. The figure shows that Shrink neither has the highest recall nor precision, but it always scores above the linear interpolation between Unrefined and Pre-shrink, which could indicate that Shrink achieves a better trade-off between precision and recall.

TABLE II
ABLATION STUDIES WITH DEEPCRACK AS THE MACRO BRANCH. **BOLDED** AND <u>UNDERLINED</u> VALUES INDICATE THE BEST AND SECOND BEST
PERFORMING SETTINGS, RESPECTIVELY.

|	Aigle				CFD				DCD			
	R	R-er	Dil-1	Dil-4	R	R-er	Dil-1	Dil-4	R	R-er	Dil-1	Dil-4
w/o Micro Branch	0.594	0.563	0.626	0.465	0.649	0.629	0.628	0.549	0.840	0.837	0.832	0.808
w/o Annotation Refinement [6]	**0.816**	**0.808**	<u>0.772</u>	**0.775**	0.629	0.590	0.636	0.574	0.835	0.830	0.831	0.823
w/o Ignore Condition	0.730	0.673	0.736	0.688	0.630	<u>0.643</u>	0.637	0.595	0.842	<u>0.846</u>	0.837	<u>0.836</u>
w/o Shrink	0.748	0.738	0.733	0.727	<u>0.650</u>	0.637	**0.651**	**0.617**	<u>0.847</u>	0.840	<u>0.840</u>	**0.840**
Proposed	<u>0.778</u>	<u>0.761</u>	**0.776**	<u>0.765</u>	**0.658**	**0.644**	<u>0.646</u>	<u>0.596</u>	**0.849**	**0.852**	**0.844**	<u>0.836</u>
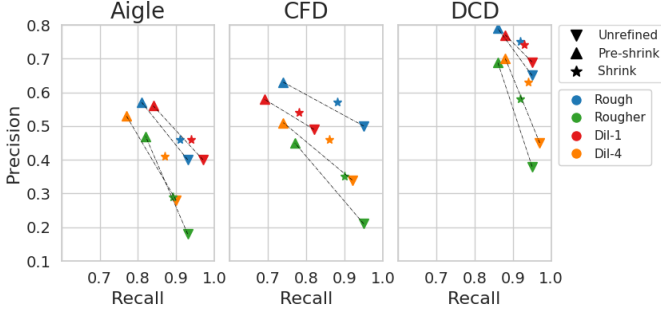
Fig. 10. Annotation qualities of different refinement methods. The loss in recall introduced by the Myopic Models (*Pre-shrink*) is recovered after the shrink operation, and it is better than a simple linear interpolation between Pre-shrink and Unrefined.

Fig. 11. Comparisons between in-domain (<u>underlined</u>), out-of-domain (*italicized*), and weakly-supervised (regular font) results for different models.

B. Weakly-Supervised vs. Model Reuse

We claimed in Sec. I that it is more favorable to collect new sets of annotations at each site, as the appearance of a crack varies greatly. In fact, the assumption that crack detectors do not generalize well across different locations is one of the biggest motivations of this work. In this section, we empirically confirm this claim by training the models on the Precise Annotation and evaluating them on various datasets. For the rest of the paper, cases in which train and test datasets match will be referred to as in-domain (*ID*), and cases in which train and test datasets do not match will be referred to as out-of-domain (*OOD*).

Fig. 11 summarizes the change in ODS for OOD results (italicized) with respect to the ID result (underlined) that share the same test dataset in each row. In other words, values in the same row are compared, with positive values corresponding to

performance improvement for training on different datasets or annotations. All results (including OOD inferences) are refined with the Micro Branch for a fair comparison.

In order to investigate whether model reuse is an effective strategy, we must find a pair of training data and the Macro Branch model architecture that does not drop in performance when it is evaluated with an OOD dataset. For example, if we train DeepCrack with CFD, the performance drops by 0.039 and 0.463 compared to the ID cases, which means that this pair is not suitable for model reuse. As it turns out, the results show that most pairs lead to poor results for at least one OOD test dataset, and thus are not suitable for model reuse. The only exception is the MIL-CD/Aigle pair, with its relatively mild OOD performance drops of 0.023 and 0.027 for CFD and DCD, respectively. Interestingly, many models seem to generalize better when trained with Aigle, the smallest dataset. This is counter-intuitive, as larger datasets are generally assumed to generalize better. This makes it difficult to compile a dataset that trains robust models, as simply annotating more samples does not equate to robustness.

Although the MIL-CD/Aigle pair may seem like the answer to domain shift, we are skeptical of its robustness for two reasons. First, there is a chance that this is a case of a multiple comparisons problem- because there are so many model/train dataset pairs, one of the pairs may achieve high performance by chance. In fact, when we analyze the pair separately, another story emerges- MIL-CD drops in performance by a significant amount (>0.1) when it is trained with CFD or DCD, and training other models with Aigle drops performance by a significant amount (>0.1) for MIL-CD Light or DeepCrack and 0.076 for DeepLab. In other words, performance drop mitigation is not consistent. Second, the evaluated datasets exhibit relatively small domain shifts compared to reality. Most public datasets are composed of roads, often void of lively colors. Therefore, it is likely that the performance drop will be worse when Aigle trained MIL-CD is evaluated on colorful buildings, for example.

Fig. 11 also summarizes the results for the weak annotations, *i.e.* the Rough and Rougher Annotations. Note that for weak annotations, train and test datasets match, and annotation refinement is applied in addition to the Micro Branch. As the figure shows, weak supervision outperforms almost all OOD performance. In fact, models trained with the Rough Annotation outperform the ID results in 7 out of the 12 cases, showing its effectiveness.
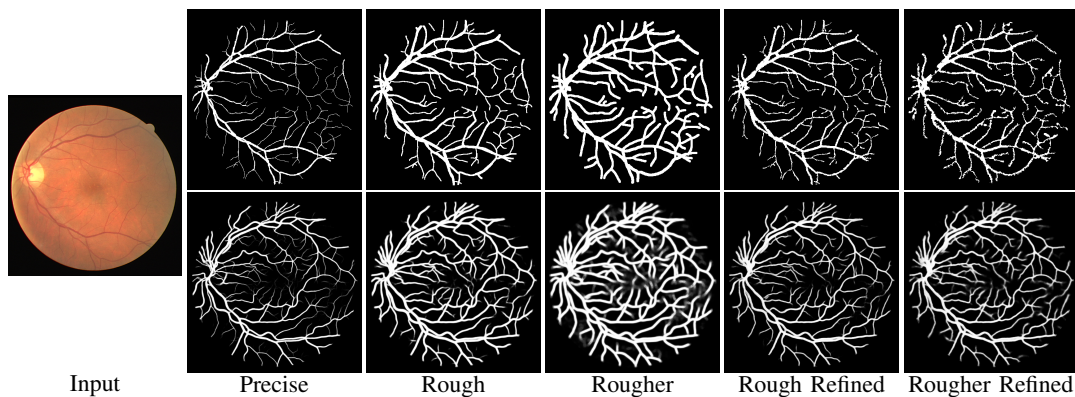
Fig. 12. Sample annotations (top row) and corresponding predictions (bottom row) of the DRIVE dataset.

TABLE III
EVALUATION OF SA-UNET [30] ON DRIVE DATASET UNDER VARIOUS
ANNOTATIONS. MIB STAND FOR THE INCLUSION OF MICRO BRANCH.

Annotation	MiB	Refined	Sensitivity	Specificity	F1
Precise			0.808	0.985	0.821
Rough			0.941	0.927	0.696
	✓		0.653	0.977	0.691
		✓	0.889	0.962	0.780
	✓	✓	0.564	0.990	0.678
Rougher			0.958	0.852	0.547
	✓		0.669	0.954	0.623
		✓	0.910	0.948	0.742
	✓	✓	0.576	0.988	0.677

After comparing the results of ID inference, OOD inference, and weak annotations, we conclude that (1) prediction accuracy significantly drops when the test and train domains do not match (2) while performance drop may be mitigated by selecting a specific training model/dataset pair, it is not clear whether they will be robust when presented to larger domain shifts (3) proposed weakly-supervised approach significantly outperforms the OOD result, and sometimes even outperforms the ID result. As the annotation cost of the proposed approach is kept minimal, we believe the large gain in accuracy and stability of the result compared to the OOD inference make our proposal an appealing option when deploying crack detectors in multiple domains.

C. Retinal Blood Vessel Segmentation

To see if the proposed refinement strategy is effective across different domains, the proposed framework is applied to the retinal blood vessel segmentation task. SA-UNet [30] is chosen as the Macro Branch for its near-state-of-the-art performance and the availability of the code, and it is evaluated on the DRIVE dataset [31], which is a popular dataset in this field. Following the annotation protocols described in Sec. IV-A1, LQ annotations of DRIVE were prepared as shown in Fig. 12. For the record, it took 3.5 hours and 1.7 hours to annotate the Rough and Rougher Annotations, respectively.

Table III summarizes the results. Note that the evaluation metrics are in accordance with the retinal blood vessel segmentation literature. For example, a single threshold value of

0.5 is used for evaluation, unlike the adaptive thresholding evaluation used in ODS. As the F1-score shows, the annotation refinement is effective for retinal blood vessel segmentation as well. This can also be observed qualitatively in Fig. 12. On the other hand, the Micro Branch performed poorly for DRIVE. This can be explained by the fact that the brightness distributions of DRIVE are strongly overlapping, as shown in Fig. 7.

The final observation is that, unlike crack detection, the results of weakly-supervised settings did not outperform the results of the fully-supervised setting. One observation regarding this point is that the models trained on LQ annotations were not good at precisely predicting narrow blood vessels. The predictions were often too thick compared to the ground truth. This is shown qualitatively by the prediction samples in Fig. 12 and quantitatively by the high sensitivity and low specificity of the models trained with LQ annotations without the Micro Branch. It is likely that Myopic Models had harder time training, as retinal blood vessel images have larger color shifts than crack images. However, we still believe that the reduction in annotation cost more than makes up for the loss in accuracy, and conclude that the proposed method is effective across different domains.

VI. CONCLUSION

This paper reformulated crack detection as a weakly-supervised problem and proposed an inference framework to counteract the loss in annotation quality. The effectiveness of the proposed framework was shown empirically- it was able to maintain accuracy even when the annotation quality was undermined. Furthermore, it significantly and consistently outperformed the out-of-domain results with a minimal annotation effort, confirming the superiority of the weakly-supervised crack detection. Furthermore, the experiments show that the proposed framework can be applied to non-crack targets, which could be an interesting topic to be pursued in the future.

APPENDIX A
RESULTS ON THE WEAKLY-SUPERVISED ANNOTATIONS

Tabular versions of Fig. 6 are provided in Table IV and Table V for precise numerical comparisons.

TABLE IV

ODS for training with the Synthetic Annotations. Integers below model names correspond to n_{dil}, the number of dilation operations applied during the data synthesis process. AR and MiB stand for Annotation Refinement and Micro Branch, respectively.

	AR	MiB	MIL-CD Light					MIL-CD					DeepCrack					DeepLab V3+				
			0	1	2	3	4	0	1	2	3	4	0	1	2	3	4	0	1	2	3	4
Aigle			0.477	0.501	0.434	0.419	0.416	0.725	0.516	0.468	0.407	0.366	0.724	0.579	0.483	0.411	0.323	0.616	0.511	0.465	0.409	0.408
		✓	0.691	0.788	0.787	0.776	0.768	0.803	0.806	0.800	0.796	0.775	0.787	0.772	0.781	0.789	0.774	0.806	0.794	0.787	0.792	0.765
	✓		0.477	0.521	0.475	0.486	0.485	0.725	0.536	0.533	0.495	0.461	0.724	0.625	0.555	0.537	0.465	0.616	0.567	0.535	0.492	0.476
	✓	✓	0.691	0.786	0.795	0.788	0.772	0.803	0.802	0.804	0.804	0.796	0.787	0.776	0.780	0.765	0.765	0.806	0.830	0.814	0.808	0.782
CFD			0.587	0.602	0.557	0.517	0.498	0.678	0.627	0.583	0.555	0.533	0.657	0.603	0.54	0.501	0.445	0.667	0.635	0.516	0.431	0.372
		✓	0.623	0.610	0.586	0.567	0.557	0.670	0.615	0.588	0.572	0.558	0.656	0.636	0.601	0.588	0.574	0.666	0.628	0.592	0.575	0.563
	✓		0.587	0.625	0.611	0.588	0.580	0.678	0.644	0.640	0.622	0.611	0.657	0.628	0.615	0.595	0.549	0.667	0.661	0.627	0.590	0.553
	✓	✓	0.623	0.623	0.609	0.601	0.587	0.670	0.628	0.619	0.609	0.598	0.656	0.646	0.633	0.625	0.596	0.666	0.647	0.621	0.604	0.589
DCD			0.782	0.756	0.699	0.698	0.640	0.795	0.783	0.734	0.709	0.674	0.841	0.799	0.776	0.769	0.749	0.842	0.786	0.764	0.685	0.642
		✓	0.824	0.821	0.813	0.810	0.805	0.822	0.831	0.822	0.817	0.813	0.845	0.831	0.824	0.833	0.823	0.848	0.818	0.825	0.817	0.797
	✓		0.782	0.790	0.777	0.772	0.766	0.795	0.802	0.797	0.784	0.763	0.841	0.832	0.822	0.815	0.808	0.842	0.820	0.809	0.794	0.764
	✓	✓	0.824	0.823	0.830	0.830	0.826	0.822	0.833	0.833	0.830	0.827	0.845	0.844	0.844	0.840	0.836	0.848	0.831	0.830	0.818	0.810

TABLE V

ODS for training with the Rough and Rougher Annotations.

	AR	MiB	MIL-CD Light			MIL-CD			DeepCrack			DeepLab V3+		
			Precise	Rough	Rougher	Precise	Rough	Rougher	Precise	Rough	Rougher	Precise	Rough	Rougher
Aigle			0.477	0.433	0.383	0.725	0.522	0.435	0.724	0.538	0.410	0.616	0.487	0.407
		✓	0.691	0.773	0.781	0.803	0.816	0.802	0.787	0.816	0.808	0.806	0.773	0.811
	✓		0.477	0.548	0.493	0.725	0.522	0.534	0.724	0.594	0.563	0.616	0.519	0.559
	✓	✓	0.691	0.783	0.782	0.803	0.800	0.809	0.787	0.778	0.760	0.806	0.815	0.804
CFD			0.587	0.586	0.519	0.678	0.625	0.588	0.657	0.624	0.536	0.667	0.649	0.506
		✓	0.623	0.621	0.591	0.670	0.631	0.597	0.656	0.629	0.590	0.666	0.641	0.599
	✓		0.587	0.633	0.598	0.678	0.644	0.632	0.657	0.649	0.628	0.667	0.649	0.629
	✓	✓	0.623	0.629	0.611	0.670	0.641	0.621	0.656	0.658	0.644	0.666	0.643	0.622
DCD			0.782	0.770	0.701	0.795	0.796	0.722	0.841	0.813	0.794	0.842	0.825	0.710
		✓	0.824	0.824	0.811	0.822	0.836	0.813	0.845	0.835	0.830	0.848	0.842	0.823
	✓		0.782	0.799	0.781	0.795	0.806	0.774	0.841	0.840	0.837	0.842	0.824	0.825
	✓	✓	0.824	0.831	0.818	0.822	0.837	0.833	0.845	0.849	0.852	0.848	0.843	0.833

Appendix B
Test-Train Split for Aigle and CFD

Although both Aigle and CFD are well-known public datasets used in many crack detection literature, we were not able to find any official test-train split for those datasets. So we record our split in this section to promote future research.

a) Aigle Test Data: C18bor, E17aor, E17bor, F01aor, F02aor, F04bor, F05bor, F08bor, F09aor, F10bor, F12bor, F13aor, F14aor, F16aor.

b) CFD Test Data: 002, 004, 005, 006, 014, 016, 018, 024, 025, 027, 028, 029, 033, 036, 037, 038, 041, 044, 047, 049, 053, 059, 060, 062, 064, 066, 073, 074, 076, 077, 078, 085, 090, 091, 093, 094, 096, 098, 102, 104, 108, 110, 111, 112, 114, 116, 118.

References

[1] Y. Inoue and H. Nagayoshi, "Deployment conscious automatic surface crack detection," in *WACV*. IEEE, 2019, pp. 686–694.

[2] F. Yang, L. Zhang, S. Yu, D. Prokhorov, X. Mei, and H. Ling, "Feature pyramid and hierarchical boosting network for pavement crack detection," *IEEE Transactions on Intelligent Transportation Systems*, 2019.

[3] Y. Liu, J. Yao, X. Lu, R. Xie, and L. Li, "Deepcrack: A deep hierarchical feature learning architecture for crack segmentation," *Neurocomputing*, vol. 338, pp. 139–153, 2019.

[4] J.-M. Guo, H. Markoni, and J.-D. Lee, "Barnet: Boundary aware refinement network for crack detection," *IEEE Transactions on Intelligent Transportation Systems*, 2021.

[5] Z. Qu, W. Chen, S.-Y. Wang, T.-M. Yi, and L. Liu, "A crack detection algorithm for concrete pavement based on attention mechanism and multi-features fusion," *IEEE Transactions on Intelligent Transportation Systems*, 2021.

[6] Y. Inoue and H. Nagayoshi, "Crack detection as a weakly-supervised problem: Towards achieving less annotation-intensive crack detectors," in *ICPR*, 2020.

[7] A. Bearman, O. Russakovsky, V. Ferrari, and L. Fei-Fei, "What's the point: Semantic segmentation with point supervision," in *ECCV*. Springer, 2016, pp. 549–565.

[8] Y. Y. Boykov and M.-P. Jolly, "Interactive graph cuts for optimal boundary & region segmentation of objects in nd images," in *CVPR*, vol. 1. IEEE, 2001, pp. 105–112.

[9] C. Rother, V. Kolmogorov, and A. Blake, "" grabcut" interactive foreground extraction using iterated graph cuts," *ACM transactions on graphics (TOG)*, vol. 23, no. 3, pp. 309–314, 2004.

[10] A. Khoreva, R. Benenson, J. Hosang, M. Hein, and B. Schiele, "Simple does it: Weakly supervised instance and semantic segmentation," in *CVPR*, 2017, pp. 876–885.

[11] R. R. Selvaraju, M. Cogswell, A. Das, R. Vedantam, D. Parikh, and D. Batra, "Grad-cam: Visual explanations from deep networks via gradient-based localization," in *CVPR*, 2017, pp. 618–626.

[12] A. Kolesnikov and C. H. Lampert, "Seed, expand and constrain: Three principles for weakly-supervised image segmentation," in *ECCV*. Springer, 2016, pp. 695–711.

[13] J. Ahn, S. Cho, and S. Kwak, "Weakly supervised learning of instance segmentation with inter-pixel relations," in *CVPR*, 2019, pp. 2209–2218.

[14] A. Mujeeb, W. Dai, M. Erdt, and A. Sourin, "One class based feature

learning approach for defect detection using deep autoencoders," *Advanced Engineering Informatics*, vol. 42, p. 100933, 2019.

[15] G. Kang, S. Gao, L. Yu, and D. Zhang, "Deep architecture for high-speed railway insulator surface defect detection: Denoising autoencoder with multitask learning," *IEEE Transactions on Instrumentation and Measurement*, vol. 68, no. 8, pp. 2679–2690, 2018.

[16] J. Yu, D. Y. Kim, Y. Lee, and M. Jeon, "Unsupervised pixel-level road defect detection via adversarial image-to-frequency transform," in *2020 IEEE Intelligent Vehicles Symposium (IV)*. IEEE, 2020, pp. 1708–1713.

[17] R. Fan, M. J. Bocus, Y. Zhu, J. Jiao, L. Wang, F. Ma, S. Cheng, and M. Liu, "Road crack detection using deep convolutional neural network and adaptive thresholding," in *IEEE Intelligent Vehicles Symposium*. IEEE, 2019, pp. 474–479.

[18] J. König, M. Jenkins, M. Mannion, P. Barrie, and G. Morison, "Weakly-supervised surface crack segmentation by generating pseudo-labels using localization with a classifier and thresholding," *arXiv preprint arXiv:2109.00456*, 2021.

[19] Z. Dong, J. Wang, B. Cui, D. Wang, and X. Wang, "Patch-based weakly supervised semantic segmentation network for crack detection," *Construction and Building Materials*, vol. 258, p. 120291, 2020.

[20] L. Duan, H. Geng, J. Pang, and J. Zeng, "Unsupervised pixel-level crack detection based on generative adversarial network," in *Proceedings of the 2020 5th International Conference on Multimedia Systems and Signal Processing*, 2020, pp. 6–10.

[21] S. Mubashshira, M. M. Azam, and S. M. M. Ahsan, "An unsupervised approach for road surface crack detection," in *2020 IEEE Region 10 Symposium (TENSYMP)*. IEEE, 2020, pp. 1596–1599.

[22] G. Bradski, "The OpenCV Library," *Dr. Dobb's Journal of Software Tools*, 2000.

[23] S. van der Walt, J. L. Schönberger, J. Nunez-Iglesias, F. Boulogne, J. D. Warner, N. Yager, E. Gouillart, T. Yu, and the scikit-image contributors, "scikit-image: image processing in Python," *PeerJ*, vol. 2, p. e453, 6 2014. [Online]. Available: https://doi.org/10.7717/peerj.453

[24] S. Chambon and J.-M. Moliard, "Automatic road pavement assessment with image processing: review and comparison," *International Journal of Geophysics*, vol. 2011, 2011.

[25] Y. Shi, L. Cui, Z. Qi, F. Meng, and Z. Chen, "Automatic road crack detection using random structured forests," *IEEE Transactions on Intelligent Transportation Systems*, vol. 17, no. 12, pp. 3434–3445, 2016.

[26] P. Y. Simard, D. Steinkraus, J. C. Platt *et al.*, "Best practices for convolutional neural networks applied to visual document analysis." in *ICDAR*, vol. 3, 2003.

[27] A. Buslaev, V. I. Iglovikov, E. Khvedchenya, A. Parinov, M. Druzhinin, and A. A. Kalinin, "Albumentations: fast and flexible image augmentations," *Information*, vol. 11, no. 2, p. 125, 2020.

[28] Z. Fan, Y. Wu, J. Lu, and W. Li, "Automatic pavement crack detection based on structured prediction with the convolutional neural network," *arXiv preprint arXiv:1802.02208*, 2018.

[29] L.-C. Chen, Y. Zhu, G. Papandreou, F. Schroff, and H. Adam, "Encoder-decoder with atrous separable convolution for semantic image segmentation," in *ECCV*, 2018.

[30] C. Guo, M. Szemenyei, Y. Yi, W. Wang, B. Chen, and C. Fan, "Sa-unet: Spatial attention u-net for retinal vessel segmentation," in *ICPR*. IEEE, 2021, pp. 1236–1242.

[31] J. Staal, M. D. Abràmoff, M. Niemeijer, M. A. Viergever, and B. Van Ginneken, "Ridge-based vessel segmentation in color images of the retina," *IEEE transactions on medical imaging*, vol. 23, no. 4, pp. 501–509, 2004.

BIOGRAPHY SECTION

Yuki Inoue received the B.S. and M.S. degrees in Electrical Engineering from Stanford University, CA, USA, in 2016 and 2017, respectively. He currently works for Hitachi Ltd., Tokyo, Japan as a researcher in the field of computer vision.

Hiroto Nagayoshi received the B.E. and M.E. degrees in Electrical Engineering from Waseda University, Tokyo, Japan, in 1999 and 2001, respectively. Since 2001, he has worked in the field of pattern recognition and image recognition in Hitachi, Ltd., Tokyo, Japan. He was a visiting researcher at ETH, Zurich for one year from 2013 to 2014. He was a recipient of the 55th Okouchi Memorial Technology Award, the Excellence Prize of the 3rd Monodzukuri Nippon Grand Award, and the Encouragement Prize by Minister of Education and Science of 2011 Chubu Region Invention Award.